AD-A090 690 PURDUE UNIV LAFAYETTE IN DEPT OF GEOSCIENCES F/G 8/11
SYNTHETIC SEISMOGRAM MODELING.(U)
FEB 80 L W BRAILE N00014-75-C-0972
UNCLASSIFIED TR-1-80-ONR NL

1 OF 1
AD
A090690

END
DATE FILMED
11-80
DTIC

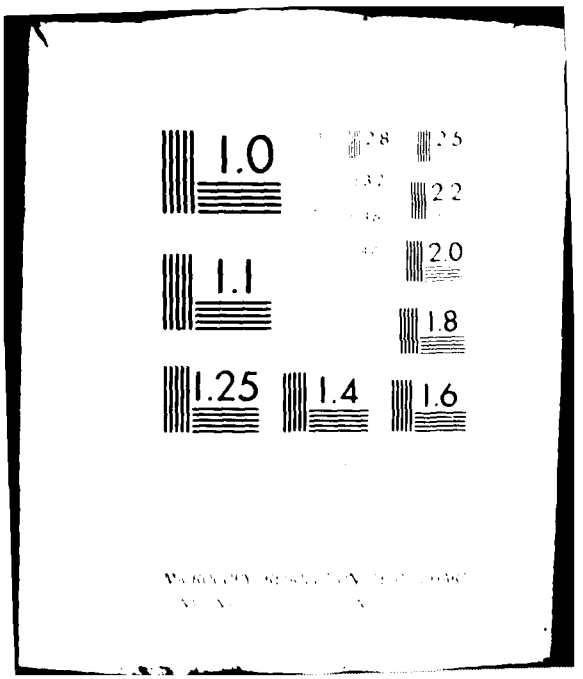
1.0
1.1
1.25
1.4
1.6
2.0
1.8

DEPARTMENT OF GEOSCIENCES
PURDUE UNIVERSITY

Technical Report
for the
EARTH PHYSICS PROGRAM
OFFICE OF NAVAL RESEARCH
Contract No. N00014-75-C-0972

SYNTHETIC SEISMOGRAM MODELING

BY

Lawrence W. Braile

Technical Report No. ONR-1-80
Project Period 5/01/79-11/30/79
Report Date 2/20/80

(9) Technical repl. 1 May - 30 Nov 79

UNCLASSIFIED

SECURITY CLASSIFICATION OF THIS PAGE (When Data Entered)

2

REPORT DOCUMENTATION PAGE

READ INSTRUCTIONS BEFORE COMPLETING FORM

1. REPORT NUMBER: ONR-1-80	2. GOVT ACCESSION NO.: AD-A090690
3. RECIPIENT'S CATALOG NUMBER:	
4. TITLE (and Subtitle): (6) Synthetic Seismogram Modeling.	5. TYPE OF REPORT & PERIOD COVERED: Technical 5/01/79 - 11/30/79
	6. PERFORMING ORG. REPORT NUMBER: ONR-1-80
7. AUTHOR(s): (10) Lawrence W. Braile	8. CONTRACT OR GRANT NUMBER(s): (15) N00014-75-C-0972
9. PERFORMING ORGANIZATION NAME AND ADDRESS: Department of Geosciences, Purdue University, West Lafayette, IN 47907	10. PROGRAM ELEMENT, PROJECT, TASK AREA & WORK UNIT NUMBERS: (11) 30 Pol 20
11. CONTROLLING OFFICE NAME AND ADDRESS: ONR Resident Representative, Ohio State Univ. Research Center, 1314 Kinnear Road, Columbus, OH 43212	12. REPORT DATE: 2/80
	13. NUMBER OF PAGES: (12) 36
14. MONITORING AGENCY NAME & ADDRESS (if different from Controlling Office): (14) TR-1 80-ONR	15. SECURITY CLASS. (of this report): Unclassified
	15a. DECLASSIFICATION/DOWNGRADING SCHEDULE: N/A

16. DISTRIBUTION STATEMENT (of this Report)

Unlimited

This [illegible] for [illegible] distribution

17. DISTRIBUTION STATEMENT (of the abstract entered in Block 20, if different from Report)

Approved for public release: distribution unlimited

18. SUPPLEMENTARY NOTES

19. KEY WORDS (Continue on reverse side if necessary and identify by block number)

Synthetic Seismograms, Seismic Modeling, Amplitudes,

20. ABSTRACT (Continue on reverse side if necessary and identify by block number)

Modeling of seismic refraction and reflection data utilizing travel-time, amplitude and synthetic seismogram methods is being investigated. State of the art techniques for both one- and two-dimensional seismic velocity models are being developed and applied to model studies. It is observed that amplitude effects are prominent and diagnostic features of the fine structure of one-dimensional models and of the lateral velocity structure in two-dimensional models. Techniques for the efficient calculation of

DD FORM 1 JAN 73 1473 EDITION OF 1 NOV 65 IS OBSOLETE

S/N 0102-LF-014-6601

SECURITY CLASSIFICATION OF THIS PAGE (When Data Entered)

409336

ABSTRACT

Modeling of seismic refraction and reflection data utilizing travel-time, amplitude and synthetic seismogram methods is being investigated. State of the art techniques for both one- and two-dimensional seismic velocity models are being developed and applied to model studies. It is observed that amplitude effects are prominent and diagnostic features of the fine structure of one-dimensional models and of the lateral velocity structure in two-dimensional models. Techniques for the efficient calculation of synthetic seismograms for an arbitrary two-dimensional elastic velocity model for a point compressional source or a dislocation earthquake source have been developed utilizing a finite-difference approximation to the heterogeneous elastic wave equation in two dimensions. Numerical difficulties associated with these methods have largely been overcome. However, the principal problem which remains in order to routinely apply this method in modeling is that of computer time and storage constraints.

INTRODUCTION

During the past three years our research has been aimed at developing improved methods for modeling seismograms - particularly those which display effects of laterally inhomogeneous velocity structure. Our approach has emphasized the development of computer codes for the calculation of synthetic seismograms. We have used analytical techniques for calculation of travel-times in homogeneous dipping or plane layers, and the Reflectivity (Fuchs and Mueller, 1971) as modified by Kind (1976, 1978), Ray tracing for the calculation of travel-times and amplitudes through 2-D structures (using techniques described

by Cerveny et al., 1978, and a program provided by Dr. Mark Odegard) and finite difference synthetic seismograms calculated for elastic and acoustic 2-D models from either a point or a dislocation (fault) source.

TRAVEL TIME CALCULATIONS IN PLANE AND DIPPING HOMOGENEOUS LAYERS

A computer program for calculating and plotting both refracted (head wave) and reflected (subcritical and supercritical or wide angle) seismic arrivals (phases) for a model consisting of plane or dipping homogeneous layers has been developed. Travel times for the head waves are given analytically and are easily determined, as is well-known. However, the reflected travel times require a numerical iterative procedure to solve the parametric time and distance equations to calculate the travel time at each desired distance. An example of the results of this program is shown in Figure 1.

MODIFIED REFLECTIVITY METHOD SYNTHETIC SEISMOGRAMS

We have extensively used the reflectivity method for calculating synthetic seismograms for a 1-D model (velocity varies only as a function of depth). Recently this method has been modified and improved by Rainer Kind and further improved and documented by us. The program utilizes the reflectivity method as previously, but now allows inclusion of (1) a compressional or a double couple (earthquake) source at any depth, (2) calculation of all wave types (for P and SV motion) including reflected and refracted P and S waves and Rayleigh waves, (3) the consideration of absorption by introducing attenuation (Q^{-1}) to each layer, (4) correct treatment of the free surface which results in prominent multiple reflected energy.

An example of the use of the modified reflectivity method to a study of the velocity structure of the Moho discontinuity is shown in Figures 2-7. Synthetic

seismograms were calculated using the modified reflectivity method for the models shown in Figure 2 which illustrate possible velocity depth curves for the Moho varying from a first order discontinuity (FOD) to a linear gradient transition with a depth range of 2, 5 and 10 km. The synthetic seismograms are shown in Figures 3-6. The primary Moho arrivals are present in the distance range of 80-240 km. P_n is a very weak first arrival beyond about 140 km with an apparent velocity of about 7.8 km/sec (negative slope on the reduced-time record sections). The P_n arrivals are somewhat masked by numerical noise in model Moho 1 - the FOD Moho model. The PmP phase is the prominent reflected arrival which follows P_n by 1-2 seconds in the range of 160-240 km.

The amplitudes of the P_n and PmP phases for the four synthetic seismograms are shown in Figure 7. It is clear from Figure 7 that the amplitude data do not provide adequate information to distinguish between the FOD model and the G-2 model. However, the amplitude-distance curves can be used to recognize and distinguish the G-5 and G-10 models from the FOD model. This means that a Moho consisting of a gradient zone of about 2 km could not be recognized as being different from a first order discontinuity, but , if the Moho is a transition zone as thick as 5 or 10 km, then we could certainly see the effect in the amplitude-distance data and discover the presence of the transition zone by modeling.

An interesting and significant feature of the synthetic seismogram record sections calculated by the modified reflectivity method is the observation of significant energy in the later arrivals, such as in the distance range of 150-240 km and 1-6 seconds reduced time, which are due to multiples and P-SV converted arrivals. The presence of this energy on the synthetic records is consistent with that observed on real refraction record sections. Furthermore, while the primary arrivals (P_g, P_n, PmP, etc) display excellent phase correlations over long distances on the synthetic records, the later arrivals show very little coherency even between adjacent seismograms. This is also consistent with observations of real refraction profiles.

RAY TRACING

We are presently utilizing two ray-tracing computer programs for the calculation of travel-times through laterally inhomogeneous velocity models. One program is due to Cerveny et al (1978) and the other was written by Dr. Mark Odegard (Odegard, 1977). Examples of these programs are shown in Figures 8-10. The principal advantage of ray-tracing techniques is the ability to efficiently calculate the travel times through a complex velocity model. We are presently attempting to modify the ray-tracing programs to also calculate amplitudes. As an example of this, Figure 11 shows a simple one-dimensional model of a layer over a half-space. The half space also includes a velocity gradient. The one-dimensional model is used so that comparison can be made with more exact synthetic seismogram amplitudes from the modified reflectivity program. We have included in the amplitude calculations the effects of geometrical spreading, energy partitioning at the interfaces due to reflection and refraction and attenuation within each layer due to absorption (Q^{-1}). Figure 12 shows the results of ray tracing through the model illustrated in Figure 11. Figure 13 gives the calculated travel-time curve and Figure 14 the calculated amplitude-distance curves. We are currently attempting to confirm that the ray tracing calculation of amplitudes and synthetic seismograms with consideration of geometrical spreading, reflection and refraction coefficients and Q is a reasonable approximation to wave-theoretical methods such as reflectivity. In addition, we are attempting to utilize the Disk ray theory approach of Wiggins (Wiggins and Madrid, 1974; Wiggins, 1976) and McMechan (McMechan, 1974; McMechan and Dey-Sarkar, 1976).

PROGRESS ON FINITE DIFFERENCE SYNTHETIC SEISMOGRAM CALCULATIONS FOR INHOMOGENEOUS VELOCITY MODELS

Finite difference calculation techniques allow approximation to the heterogeneous elastic wave equation and calculation of synthetic displacement

seismograms for two-dimensional velocity models. The finite difference method allows models to be described by a grid of physical properties, P-wave velocity, S-wave velocity and density, which may vary both laterally and vertically in an arbitrary manner. Any source time function of displacement versus time may be implemented at any position within the model grid. The limit on the source is only restricted by the frequency content of the source time function. Higher frequencies require a finer grid size and in addition a small time step in the finite difference calculations. Another feature which adds versatility to the finite difference synthetic seismogram calculation method is that all wave types are atuomatically included since it is a direct (numerical) solution to the elastic heterogeneous wave equation in two-dimensions. It is relatively simple to add anelasticity to the finite difference calculations as well by employing complex seismic velocities. In addition, it would be feasible to allow for three-dimensional propagation. However, this would greatly expand the computer capacity required for the calculations and thus, we have at present restricted ourselves to two-dimensional models.

The implementation of the finite difference displacement synthetic seismogram calculations is relatively straight-forward by approximating second partial derivatives of the heterogeneous wave equations by their finite difference equivalents. Grid spacing and time step requirements must be strictly adhered to or numerical noise and numerical instability will result. But, given that grid spacing is small enough and the time step is small enough for the frequency content of the source function, the finite difference synthetic seismograms are calculated in a straight-forward way by solving U and W displacements at each grid point in the entire velocity model for each time step and the time steps are sequentially calculated for the entire lifetime of the finite difference calculation. Therefore, the difficulties in finite difference synthetic seismogram calculation reduce to the problems of computer storage and computer time. Given large computer capacity,

realistic geologic models can be approximated with a finite difference grid of velocities and realistic synthetic seismograms can be calculated for body waves and surface waves for the inhomogeneous velocity model.

We have programmed the finite difference displacement synthetic seismogram calculations for the elastic heterogeneous wave equation in two programs. One which is designed for a simple point explosive source and another which is designed for an earthquake source in which a dislocation in displacement is utilized as a source function. This dislocation may be distributed over a finite length of a fault and the fault may be oriented in any direction in the two-dimensional model. We have used some simplifying assumptions which significantly reduce the computation time and computer storage requirements for the finite difference calculations. First we have assumed the models to be perfectly elastic. Addition of an anelasticity factor by introducing complex velocities would increase computer storage by a factor of about 2 and computer time by a factor of approximately 4, however, it is relatively easy to add the consideration of anelasticity into the finite difference calculations. In addition, for many problems it is sufficient to assume a reasonable relationship between P and S wave velocities. It is particularly convenient to assume that Poisson's ratio is equal to ¼ in which case the wave equations can be simplified considerably and storage in the computer can also be minimized. In addition, the density plays a rather minimal role in determining the propagation characteristics for most realistic geological situations and, therefore, it is feasible to assume a relationship between P-wave velocity and density such as a Nafe-Drake or a Birch law between velocity and density and this also simplifies the equations and reduces storage requirements. Special boundary conditions are required at the free surface of the synthetic seismogram computational grid and at the other boundaries of the grid which are really fictitious boundaries. At the artificial boundaries we employ an absorbing boundary condition which minimizes the reflected energy from these artificial

boundaries and allows the model size to be as small as possible for a given geologic model and this increases the versatility of the method.

At each grid point and for each time step the equations for the evaluations of the U and W displacements require solution of an equation which involves approximately 140 fortran arithmetic operations. The major effort, therefore, in calculating synthetic seismograms by the finite difference method for elastic heterogeneous models is the effort spent in solving for these displacements for each point on the grid for all the various time steps. This can add up to a very large number.

As an example of the versatility of the two-dimensional finite difference synthetic seismogram technique that we have developed, synthetic seismograms have been calculated for velocity models for an earthquake source. In Figure 15 a homogeneous half-space model has been utilized, 10 seismometers are located along the free surface separated at a station spacing of 10 kilometers. The homogeneous half-space has a P-wave velocity of 6 km/sec, a shear wave velocity of 3.47 km/sec and a density of 2.52 g/cm^3. The source was a reverse fault at depth in the homogeneous half-space approximately beneath seismometer position 6. The source time function was a ramp in time with a rise time of 2 seconds. The rupture velocity was 3 km/sec and the total dislocation was a 5 meter displacement. For a shallow reverse fault source with the upper end of the fault located at 4.4 km depth and a 4.4 km fault length, synthetic seismograms are shown in Figure 16 for seismometer positions 1 through 10. The horizontal components of displacement are the U seismograms and the vertical components are the W seismograms. For this homogeneous half-space model the radiation patterns illustrated by the vertical and horizontal component motions conform to theory. Several interesting features are illustrated on the synthetic seismograms. First, a very small P-wave, a somewhat larger S-wave and a very prominent surface wave are visible particularly at large distance from the source. The Rayleigh wave has elliptical

retrograde motion as can be verified by particle motion studies of the horizontal and vertical components. A near-field static displacement is visible particularly for seismogram positions 5 and 6 close to the fault. Also, the amplitudes of the displacements show a pronounced effect of the radiation pattern of the fault source as seen by relative amplitudes at similar distances on opposite sides of the source. Because of the small size and shallow depth of the fault, the seismograms at distances greater then about 20 km appear to be from a point source.

As a further example of the homogeneous half-space model and to facilitate comparison with an inhomogeneous velocity model, synthetic seismograms were calculated for the identical homogeneous half-space as shown in Figure 15 with the exception that the fault length and depth was increased. In Figure 17, synthetic seismograms are shown for a source which consisted of a 9.6 km long fault that was located at a 12 km depth in the homogeneous half-space model shown in Figure 15. Note that the time scale for Figures 16 and 17 differ and that the seismograms in Figure 17 display some high frequency noise which is a result of the numerical calculations. This noise could be eliminated easily by decreasing the time step for the calculations, but at the cost of increased computer time. Note that the effect of the deeper source and larger fault plane has significantly affected the shape of the recorded seismograms, particularly on the vertical component. A static displacement field is still visible in the area of about 20 km on either side of the fault. A very large difference in displacement amplitude is visible particularly on the vertical component on either side of the fault due to the depth of the source and the radiation pattern.

In Figure 18, an inhomogeneous velocity model designed to be similar to a subduction zone, for example, along the western coast of South America is shown. This model is scaled identical to the homogeneous half-space model and includes seismometer positions at 10 km separation the same as the homogeneous half-space model in Figure 15. Source function and the fault parameters are the same as for Figure 17 with the exception of the rupture velocity, which for this model was

at 3.5 km per second. The variations in P-wave velocity are shown by the numbers in the figure and this inhomogeneous distribution of velocity results in significant variations in travel time for the seismic waves propagating through the model. Synthetic seismograms calculated for the model shown in Figure 18 are illustrated in Figure 19; again vertical and horizontal components are shown and some high frequency numerical noise is present on the seismograms, but does not seriously effect the characteristics of the signals. Comparison of the seismograms for the homogeneous half-space model (Figure 17) and the subduction zone model (Figure 19) clearly illustrates the significant effect of the two-dimensional velocity structure on the recorded seismograms, particularly on the ocean side of the subduction zone model, the seismograms differs significantly from the homogeneous half-space model. Detailed signal characteristics also are significantly different between the two models. On the subduction zone model, a relatively high frequency pulse is seen to propagate in the direction of the fault to seismometer position 5. Refracted energy along the upper mantle Moho is seen as small first arrivals on the ocean side of the subduction zone model. Although absorbing boundary conditions are used at the bottom and sides of the velocity model, some reflected energy is apparent at times between about 17 and 25 seconds, particularly on the ocean side of the subduction zone model where the velocities are higher and the propagation time from the source to the lower boundary and back to the surface for the reflected energy is minimized. This reflected energy could be minimized by moving the lower boundary of the model to greater depth, but of course at the cost of greater computer time and storage capacity.

As can be seen from the examples shown, finite difference synthetic seismograms for heterogeneous models can be calculated with reasonable accuracy for realistic models and sources. The primary limitation of the finite difference

method as it is presently used is the computer time that is required. In addition, we are presently limited to two-dimensional models, although it may be possible in the future to utilize three-dimensional models with improved boundary conditions along the sides of the three-dimensional grid. This would allow for proper treatment of the geometrical spreading due to a three-dimensional source and propagation. As an example of the efficiency of calculation, the model in Figure 18 for the subduction zone consisted of 300 grid points in the horizontal position and 100 grid points in the vertical direction and 1000 time steps were calculated to obtain the synthetic seismograms for 25 seconds of propagation time. Therefore, $3x10^7$ evaluations of the vertical and horizontal displacement are required. That is, $3x10^7$ calculations of displacement by the subroutine that was previously mentioned which utilized approximately 140 fortran arithmetic operations. Storage requirements for the velocity and displacement grid for the subduction zone model were about 270,000 locations. The subduction zone model required approximately 15 minutes of CDC 7600 computer time for calculation.

Further studies which are presently underway at Purdue University involve attempts to improve the efficiency of the finite difference calculations and development of a simplified acoustic heterogeneous wave equation program which is designed to be used as a first step in modeling of two-dimensional seismic data. The advantages of the acoustic equation is that it is greatly simplified compared to the elastic equation and will provide a much faster technique for initial modeling. Of course, the assumption of acoustic wave propagation is incorrect for most real earth application and, therefore, the acoustic wave program would only be used for an initial modeling tool to approximately derive the velocity distribution and then subsequent modeling with the elastic wave equation could be utilized for refinement of the model and confirmation.

REFERENCES

Cerveny, V., I.A. Molotkov, and I. Psencik, Ray Methods in Seismology, Charles University Press, Prague, 1978.

Fuchs, K. and G. Mueller, Computation of Synthetic Seismograms with the Reflectivity Method and Comparison with Observations, Geophys. J. Roy. Astr. Soc., 23, 417-433, 1971.

Kind, R., Computation of Reflection Coefficients for Layered Media, J. Geophys., 42, 191-200, 1976.

Kind, R., The Reflectivity Method for a Buried Source, J. Geophys., 44, 603-612, 1978.

McMechan, G.A., P-wave Train Synthetic Seismograms Calculated by Quantized Ray Theory, Geophys. J. R. Astr. Soc., V. 37, No. 3, 407-421, 1974.

McMechan, G.A. and S.K. Dey-Sarkar, Quantized Ray Theory for Non-Zero Focal Depths, Geophys. J. R. Astr. Soc., 1976.

Odegard, M.E., Synthetic Seismograms for Heterogeneous Media, Tans. Am. Geophys. Union, V. 58, No. 12, 1185, 1977.

Wiggins, R.A., Body Wave Amplitude Calculations-II, Geophys. J. R. Astr. Soc., V. 46, 1-10, 1976.

Wiggins, R.A. and J.A. Madrid, Body Wave Amplitude Calculations, Geophys. R. R. Astr. Soc., V. 37, 423-433, 1974.

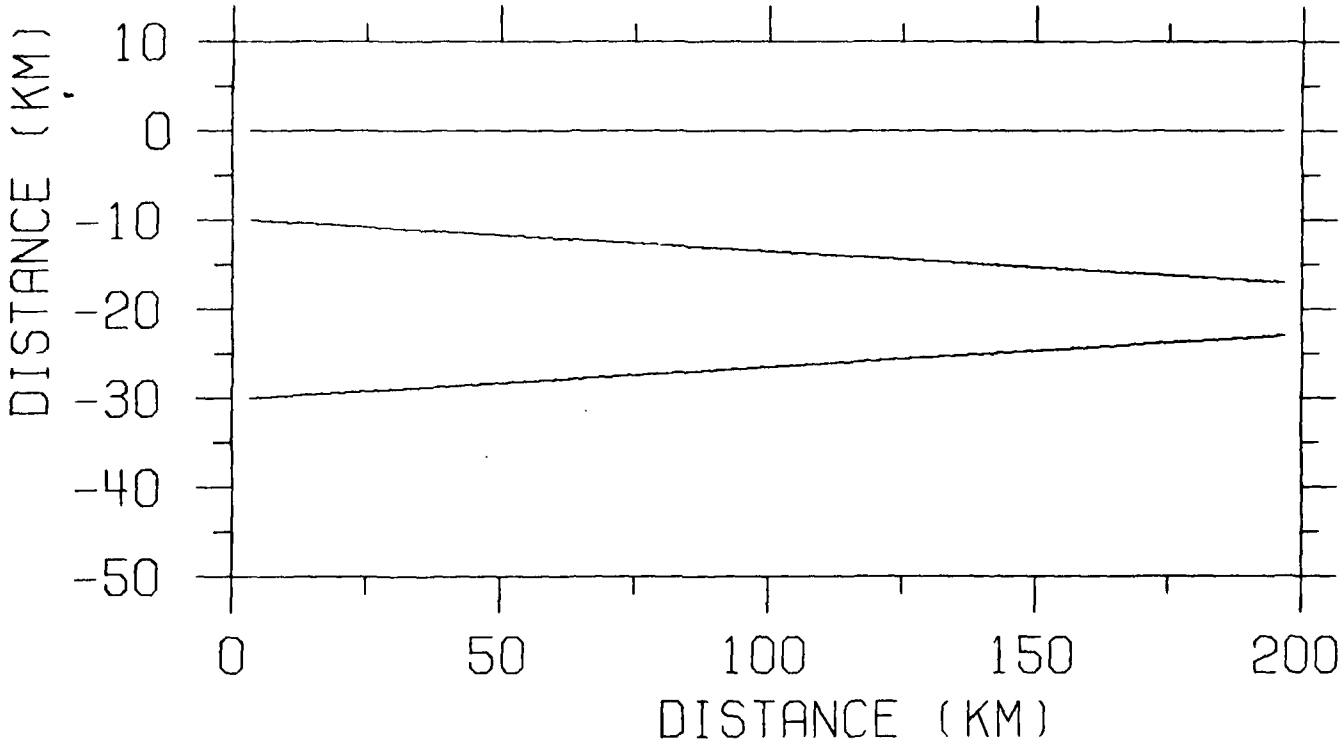

Figure 1A. Velocity model showing layer interfaces for travel-time program.

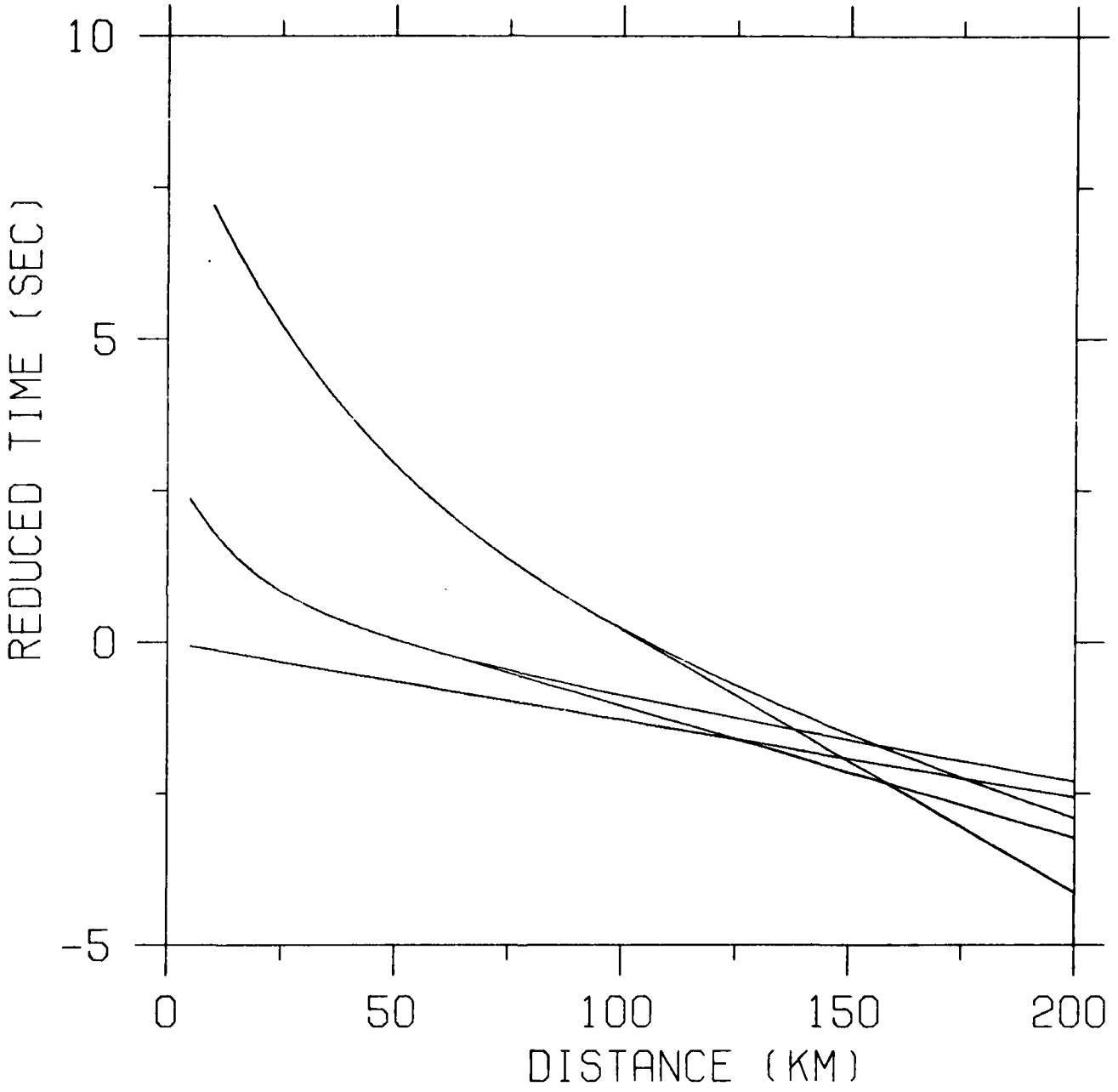

Figure 1B. Reduced travel time (T-X/6 sec) plot of reflected and refracted arrivals for the model shown in Figure 1A.

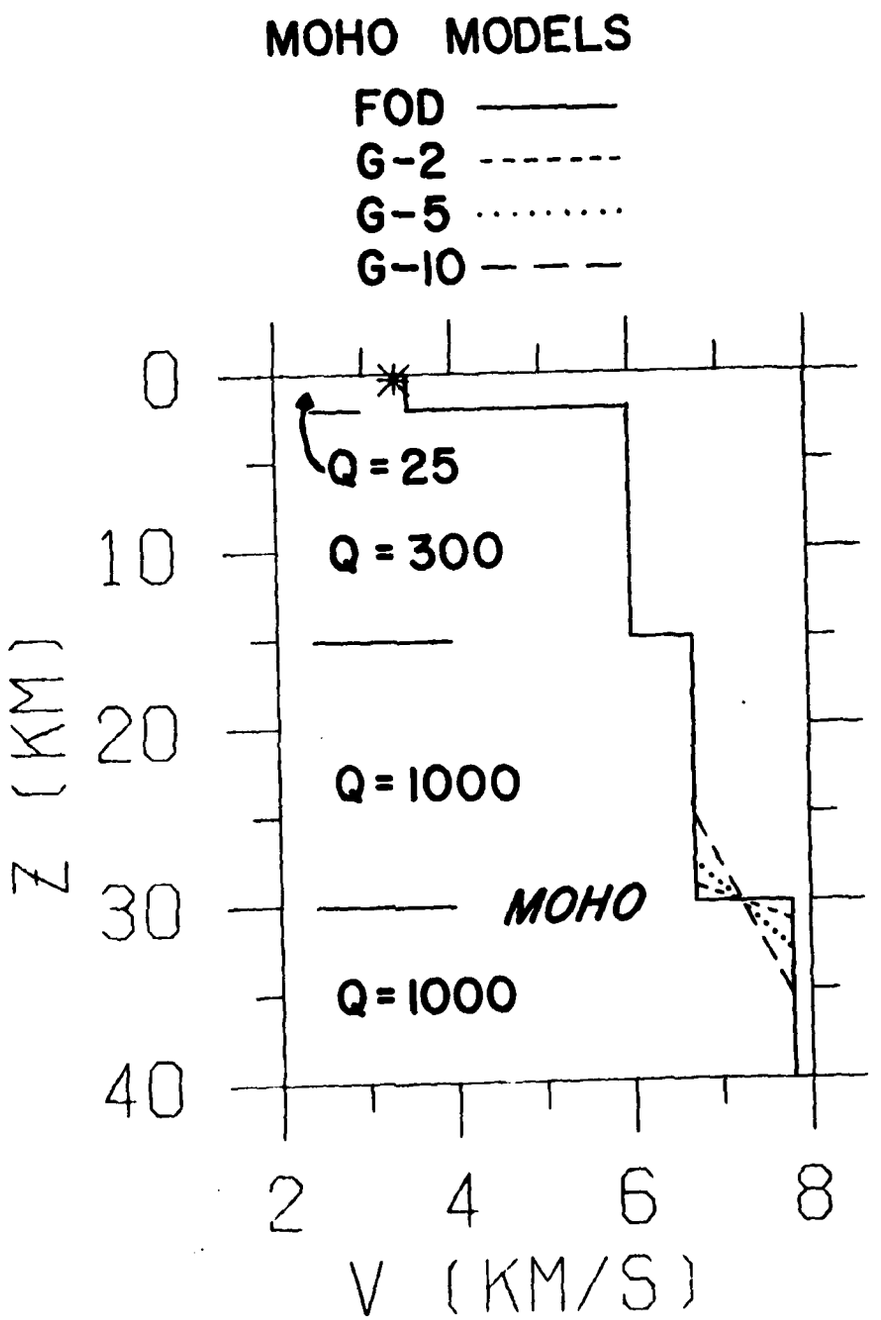

Figure 2. Velocity-depth curves for four models of the Moho. Q values for each layer are also shown.

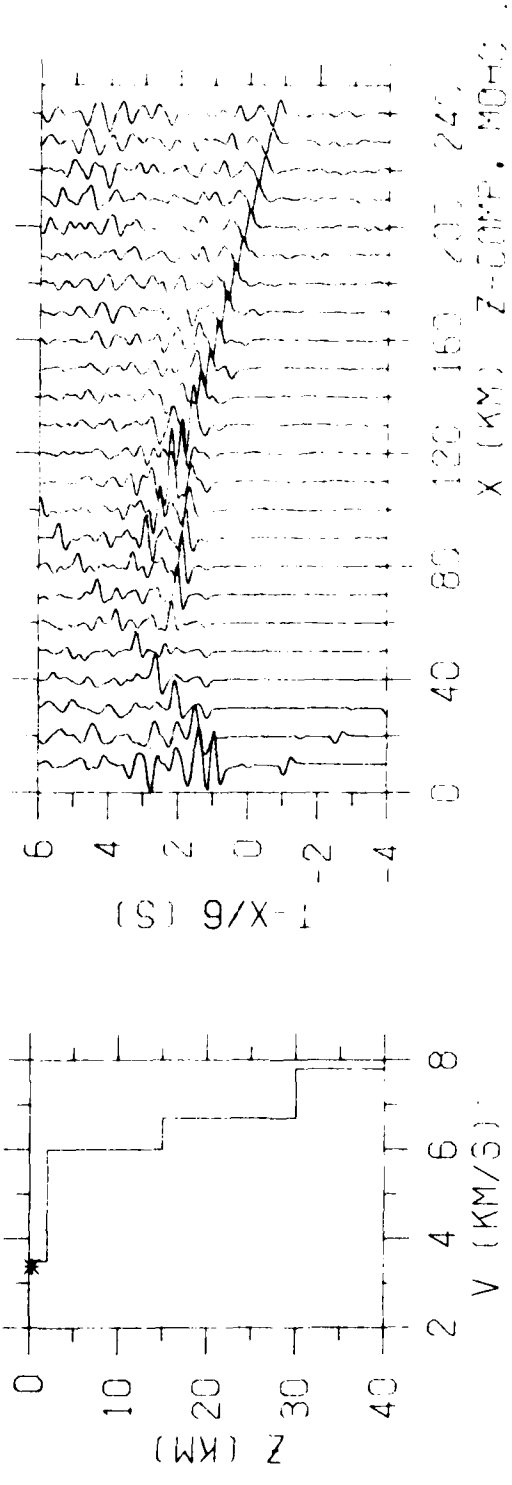

Figure 3. Synthetic seismograms (vertical component) calculated for the FOD model of Figure 2. The apparent arrivals from 10-90 km, 0 to 6 sec. reduced time, and from 10 to 30 km, -1 to -4 sec. reduced time are numerical effects and should be ignored.

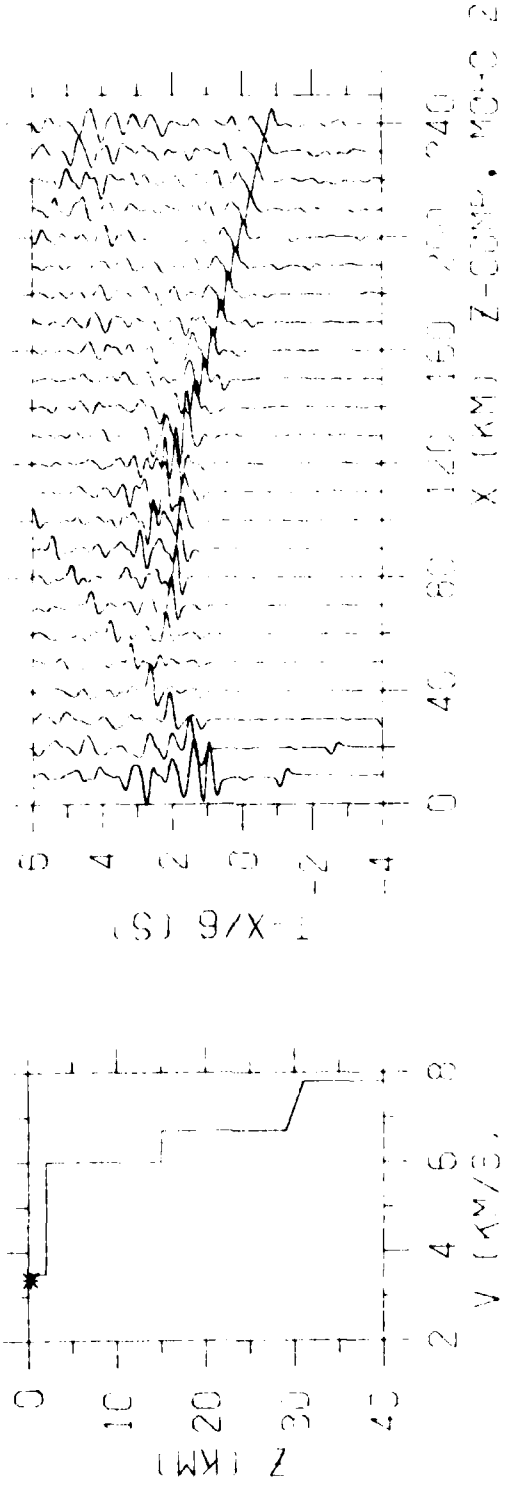

Figure 4. Synthetic seismograms (vertical component) calculated for the G-2 model of Figure 2. The apparent arrivals from 10-90 km, 0 to 6 sec. reduced time, and from 10 to 30 km, -1 to -4 sec. reduced time are numerical effects and should be ignored.

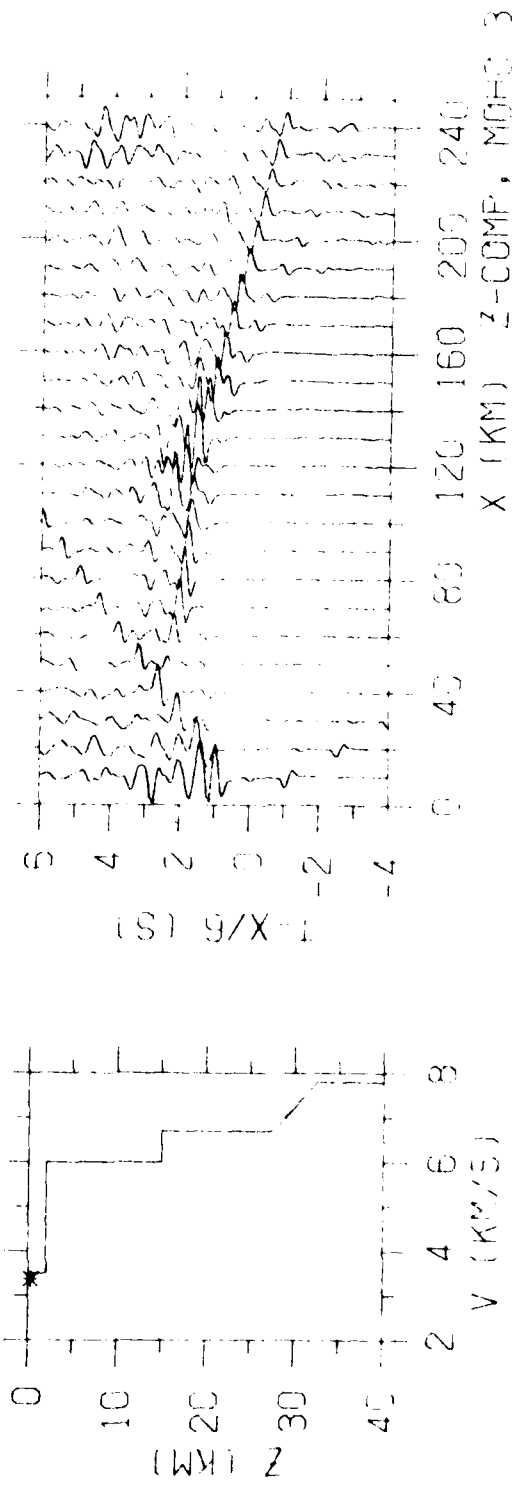

Figure 5. Synthetic seismograms (vertical component) calculated for the G-5 model of Figure 2. The apparent arrivals from 10-90 km, 0 to 6 sec. reduced time, and from 10 to 30 km, -1 to -4 sec. reduced time are numerical effects and should be ignored.

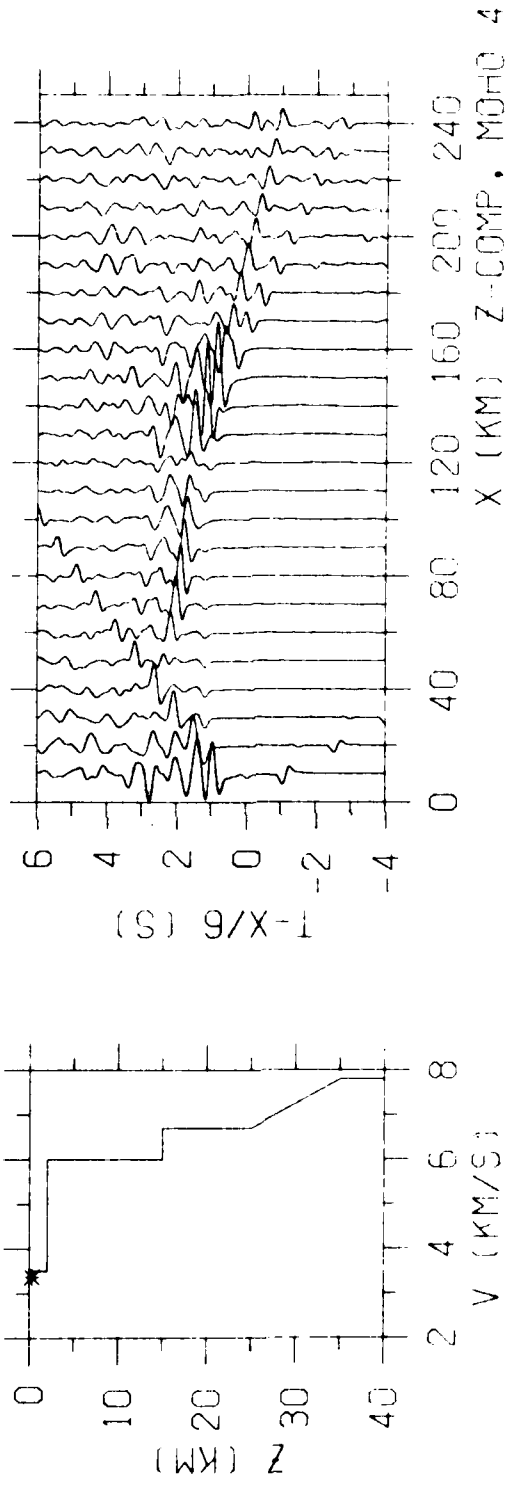

Figure 6. Synthetic seismograms (vertical component) calculated for the G-10 model of Figure 2. The apparent arrivals from 10-90 km, 0 to 6 sec. reduced time, and from 10 to 30 km, -1 to -4 sec. reduced time are numerical effects and should be ignored.

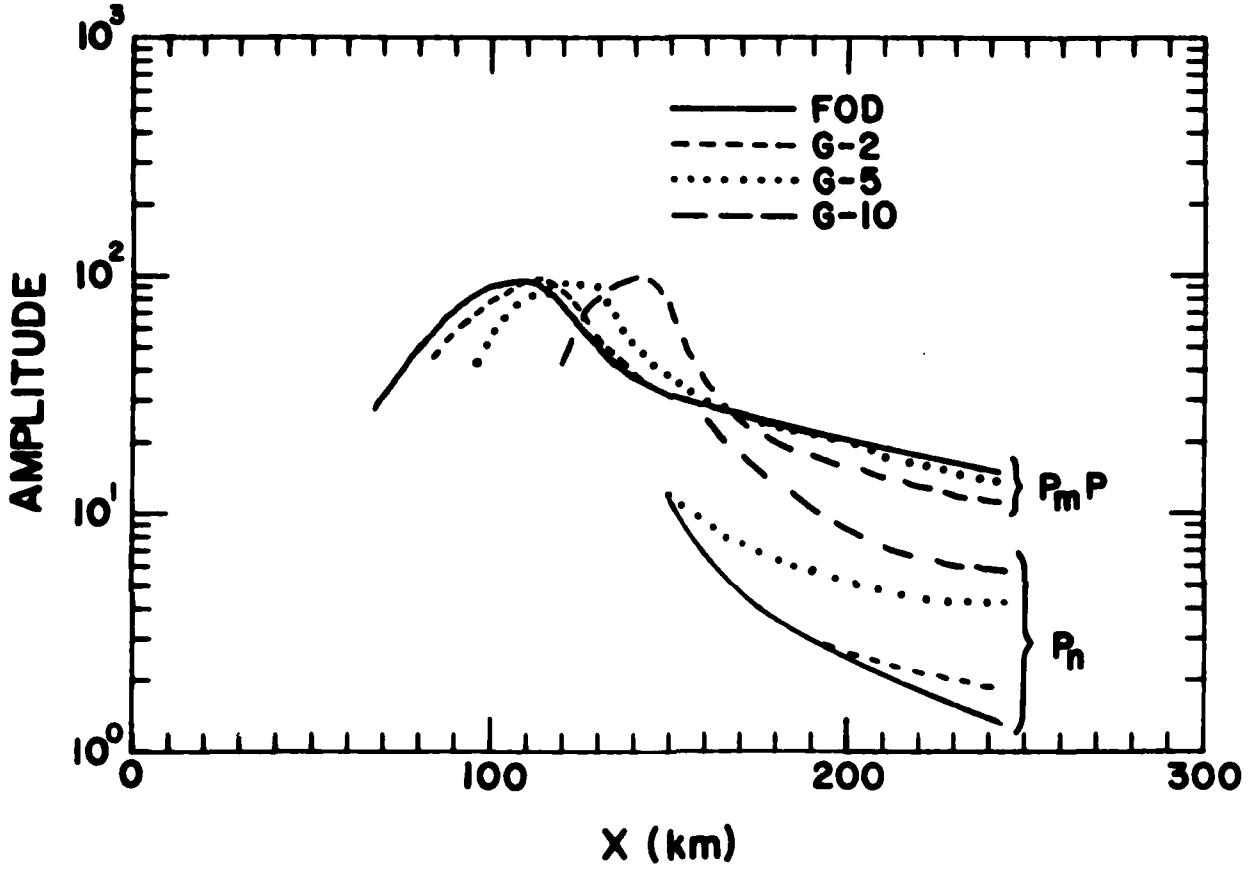

Figure 7. Amplitude-distance curves for the P_n and PmP phases for the synthetic seismograms shown in Figures 3-6.

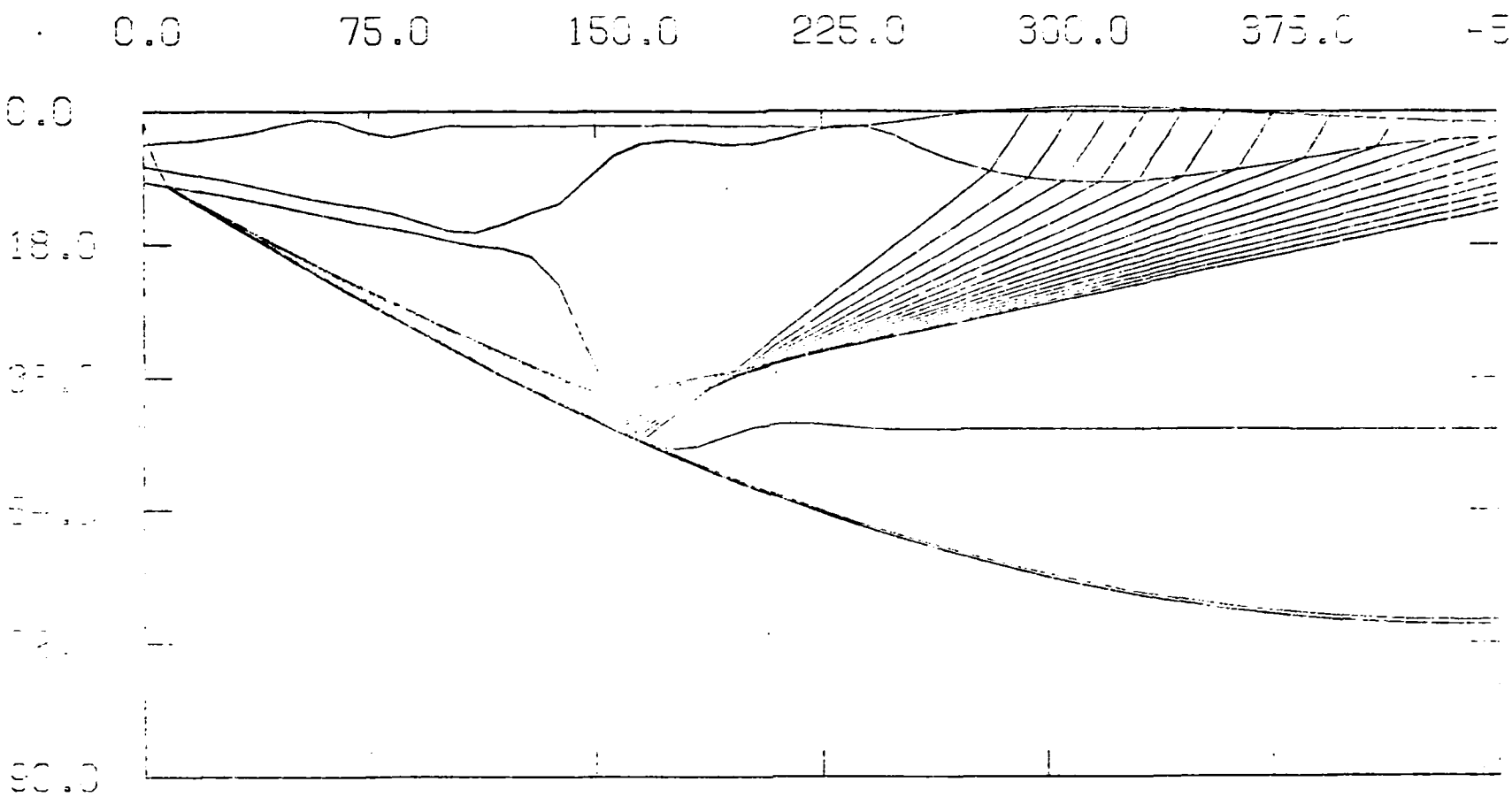

Figure 8. Ray tracing (Cerveny's method) through a laterally inhomogeneous velocity model.

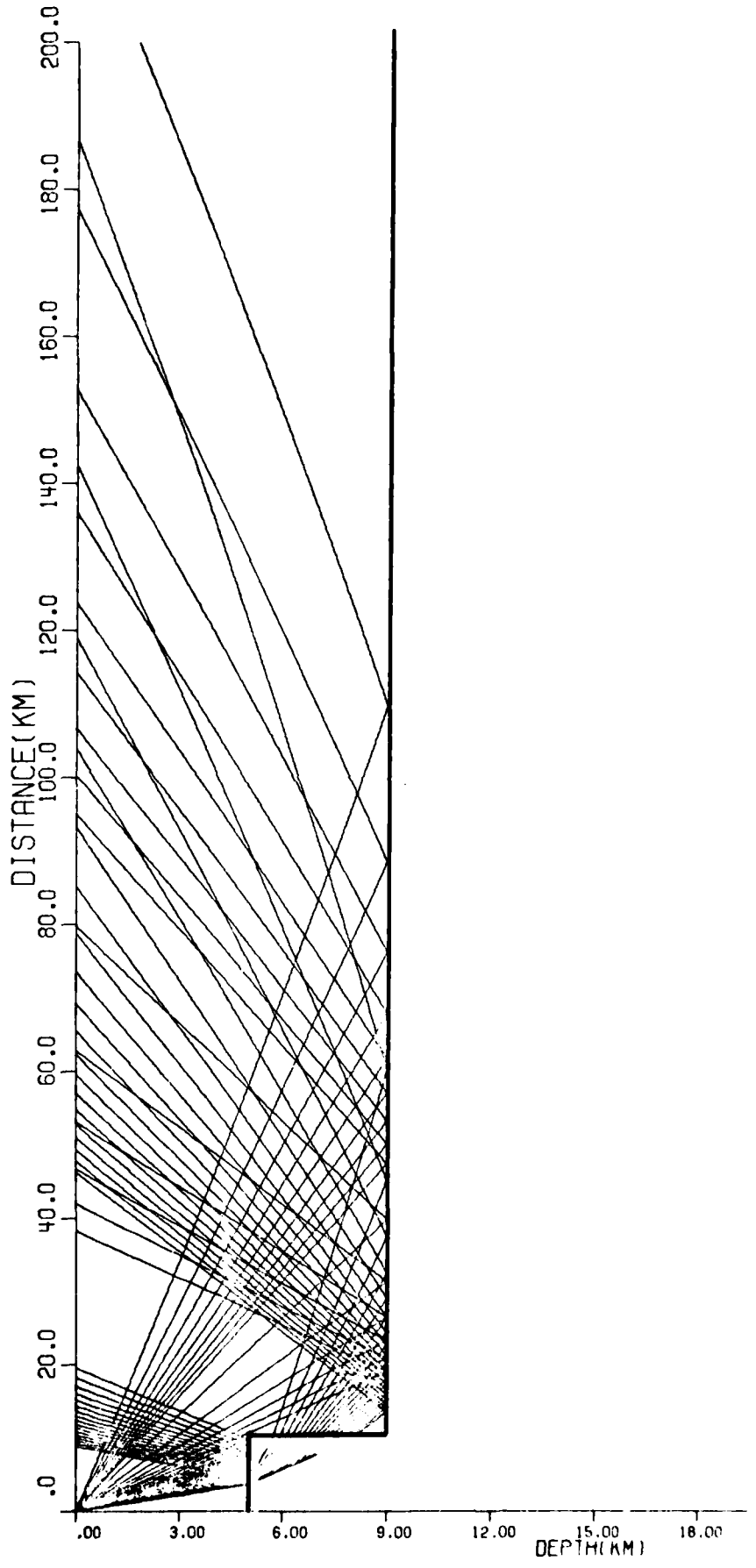

Figure 9. Ray tracing through a fault model (Odegard's Program).

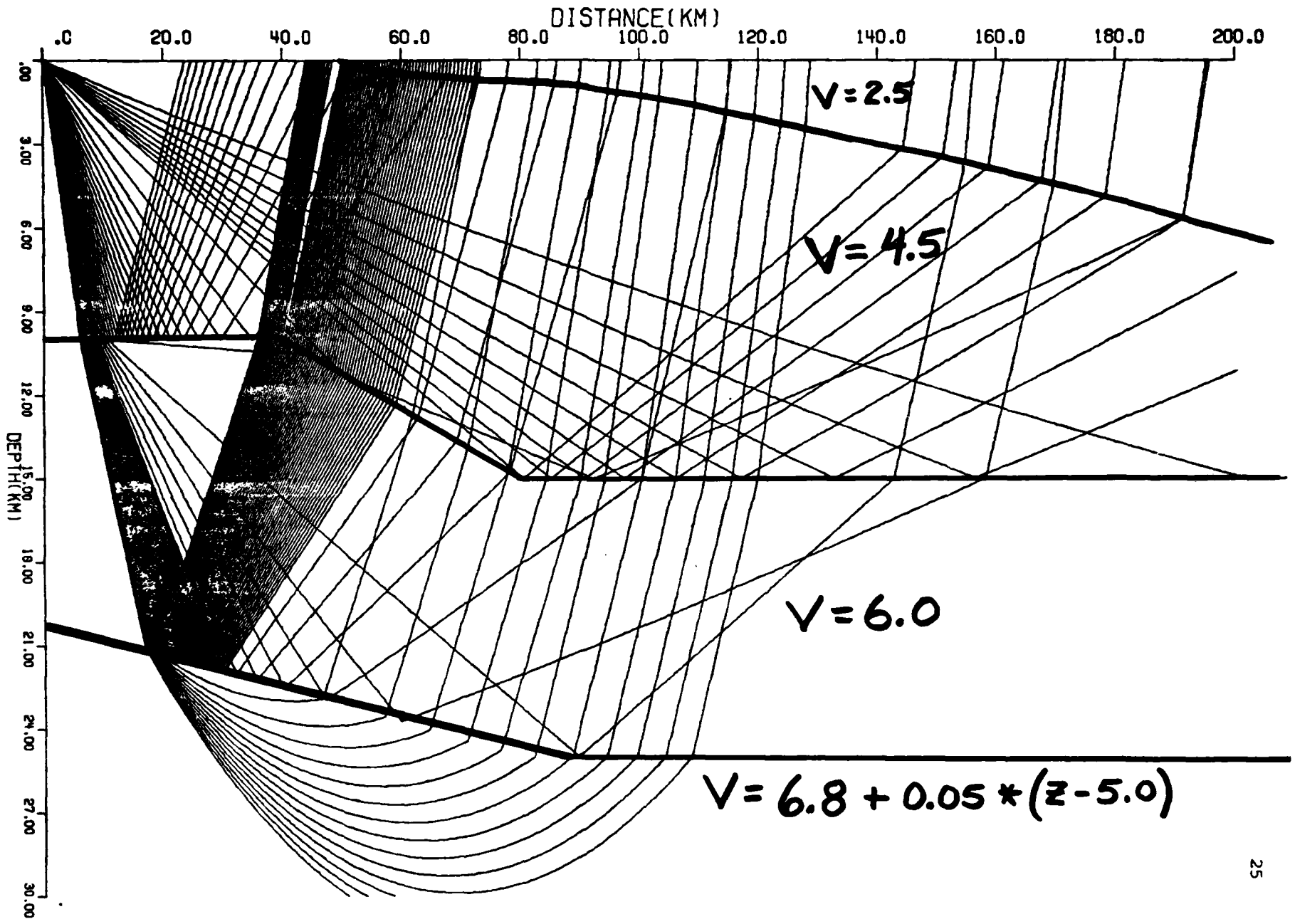

Figure 10. Ray tracing through a two-dimensional model (Odegard's program .

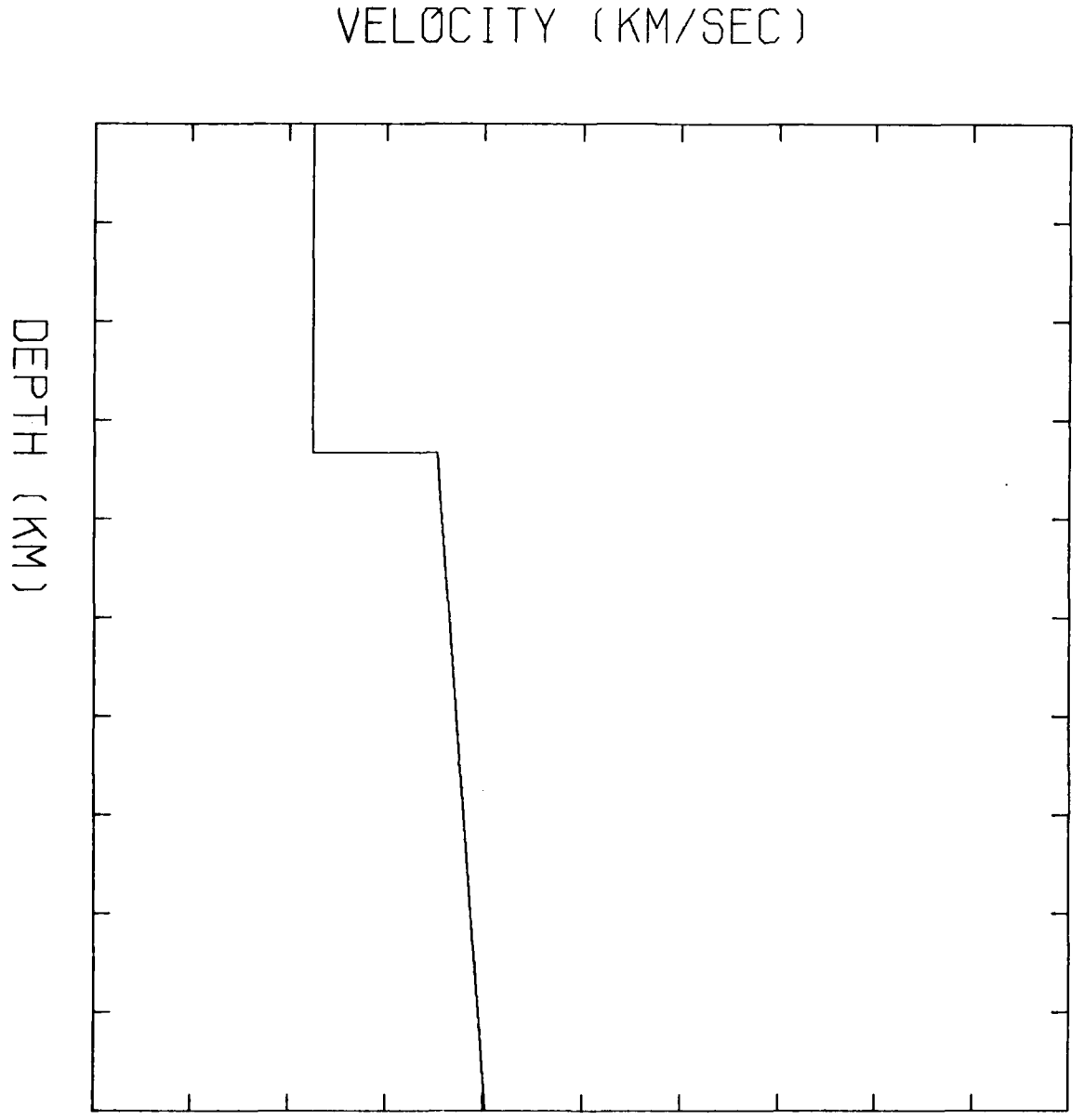

Figure 11. Velocity depth curve for layer over a half space test model.

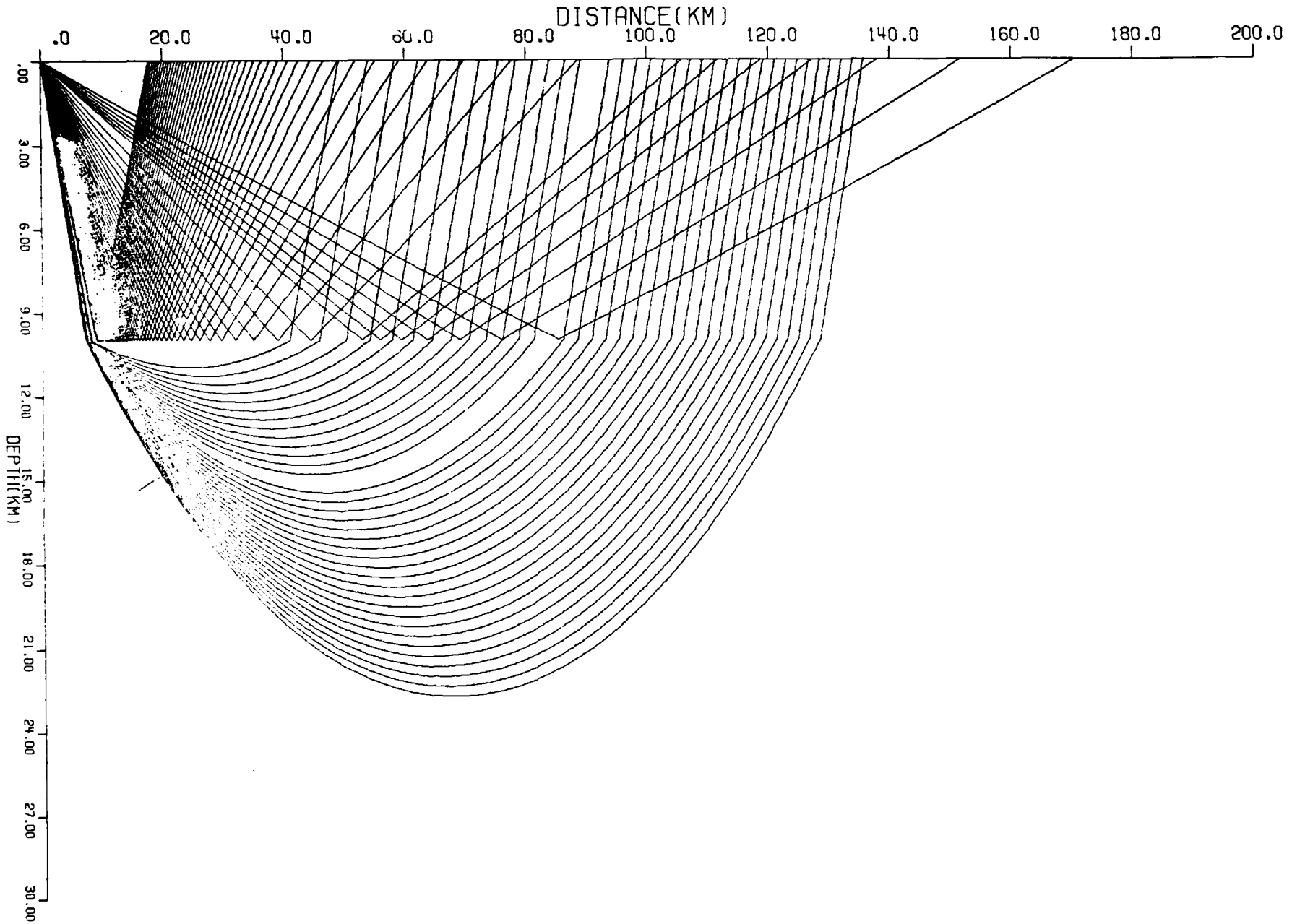

Figure 12. Ray tracing for layer over a half space test model.

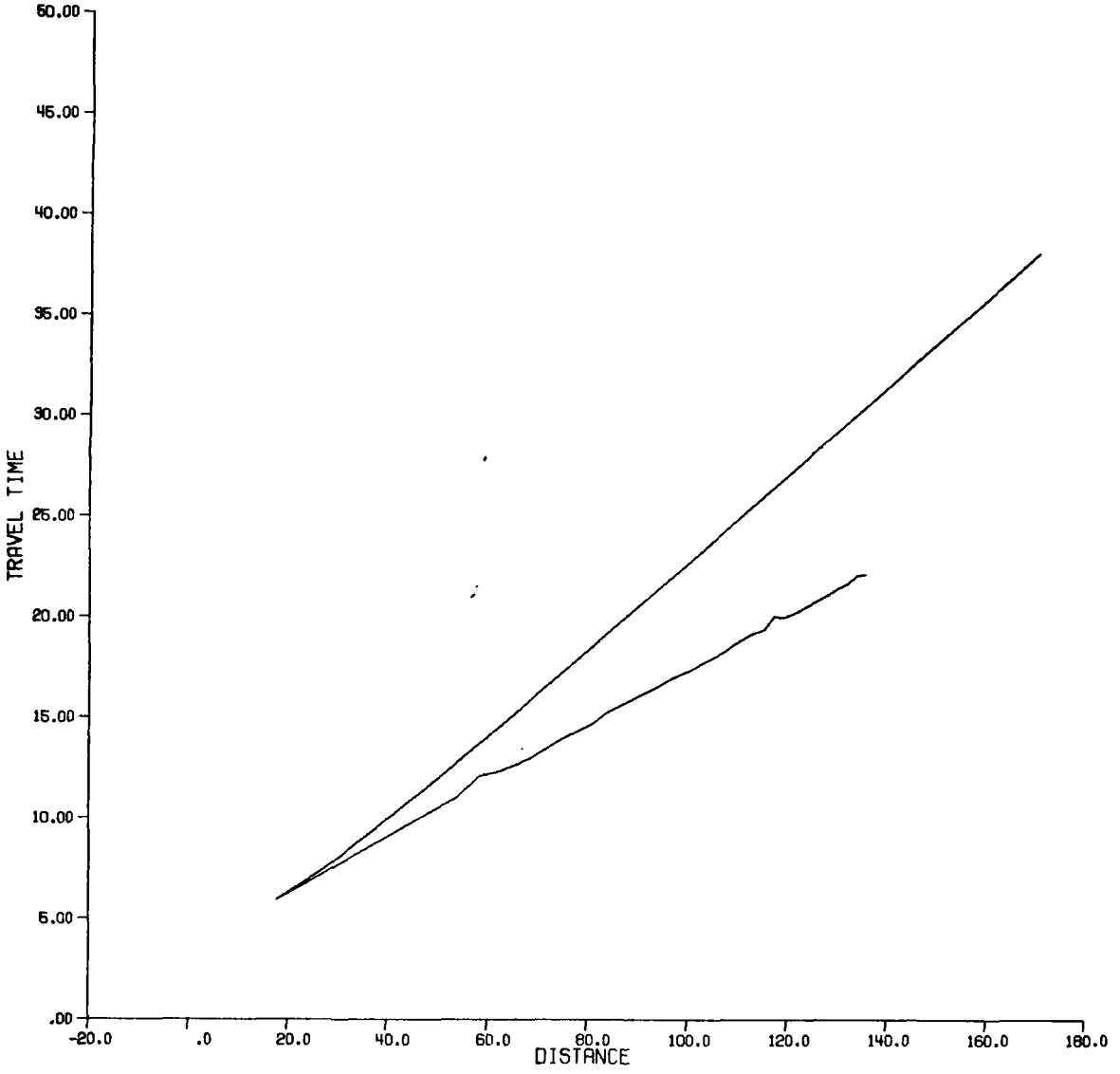

Figure 13. Travel-time curve for layer over a half space test model. Slight errors in the refracted branch travel times are numerical effects and should be ignored.

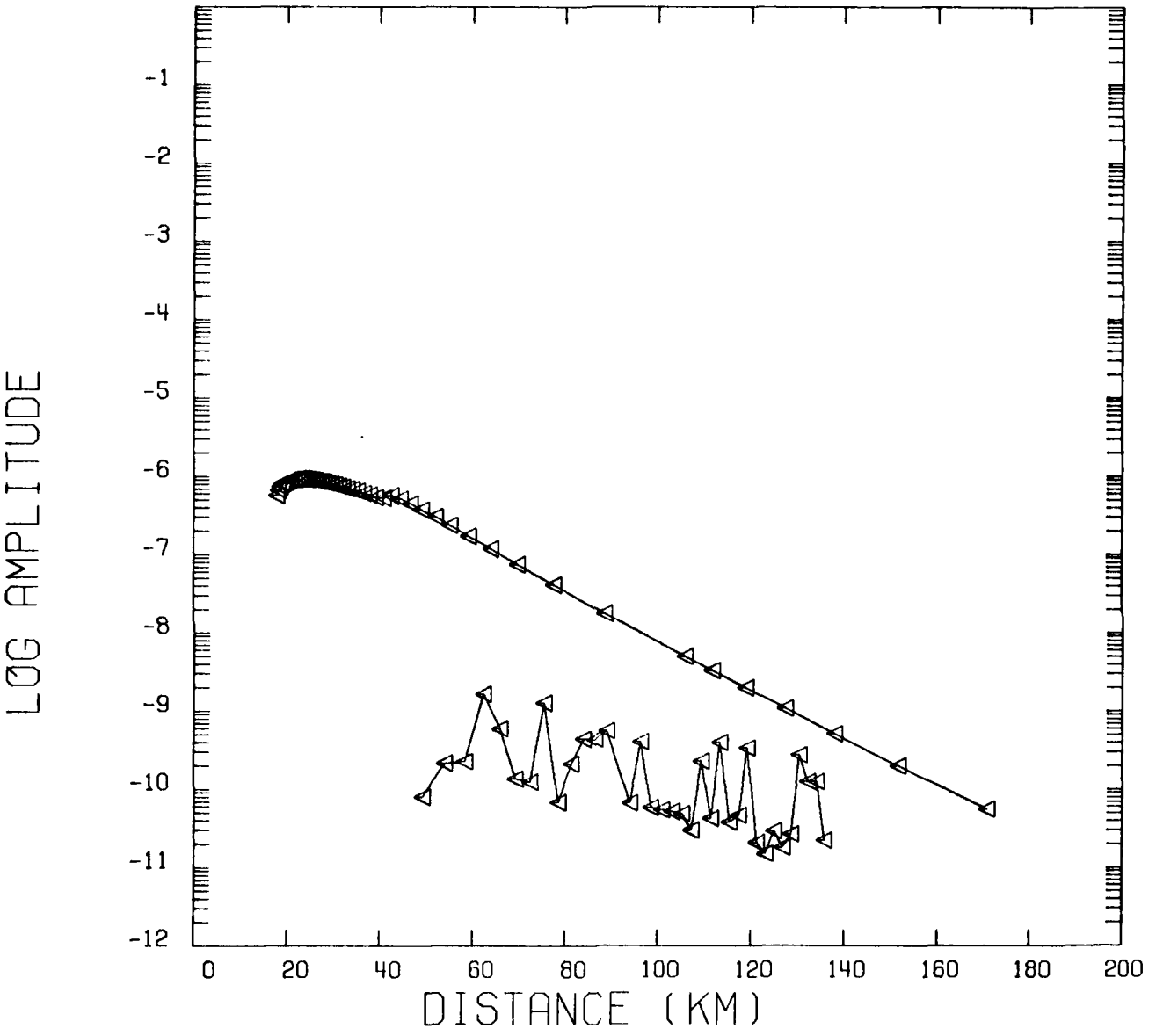

Figure 14. Amplitude-distance curve for layer over a half space test model. Upper curve is for the reflected branch and the lower curve is for the refracted branch.

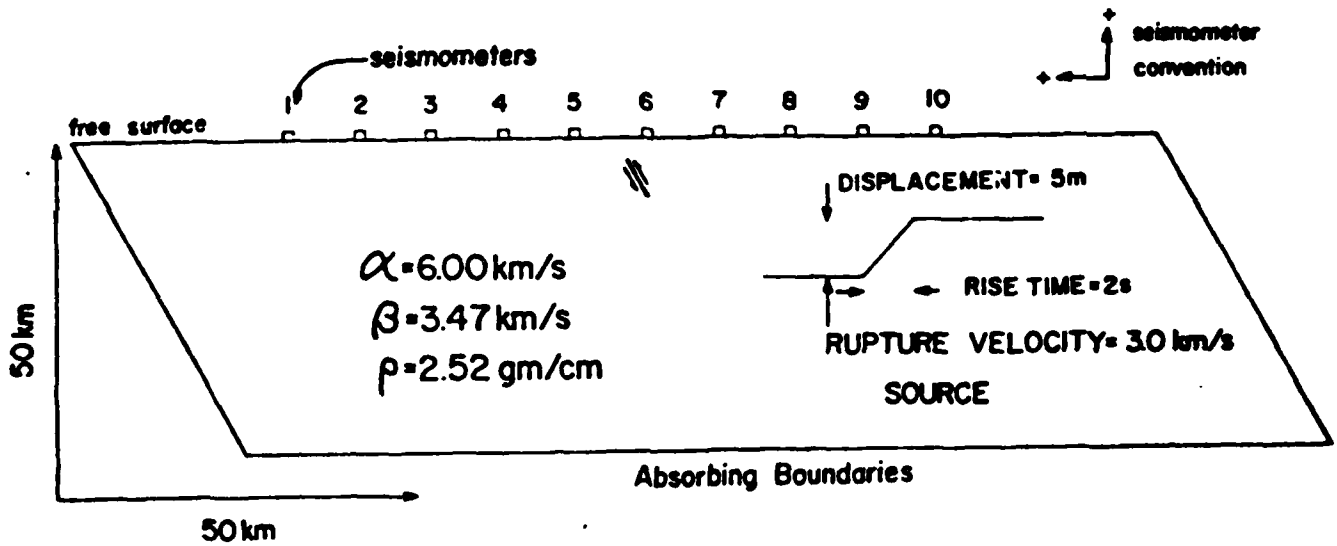

HOMOGENEOUS HALF SPACE MODEL

60° DIP REVERSE FAULT

Figure 15. Homogeneous half space model for finite difference calculation of synthetic seismograms.

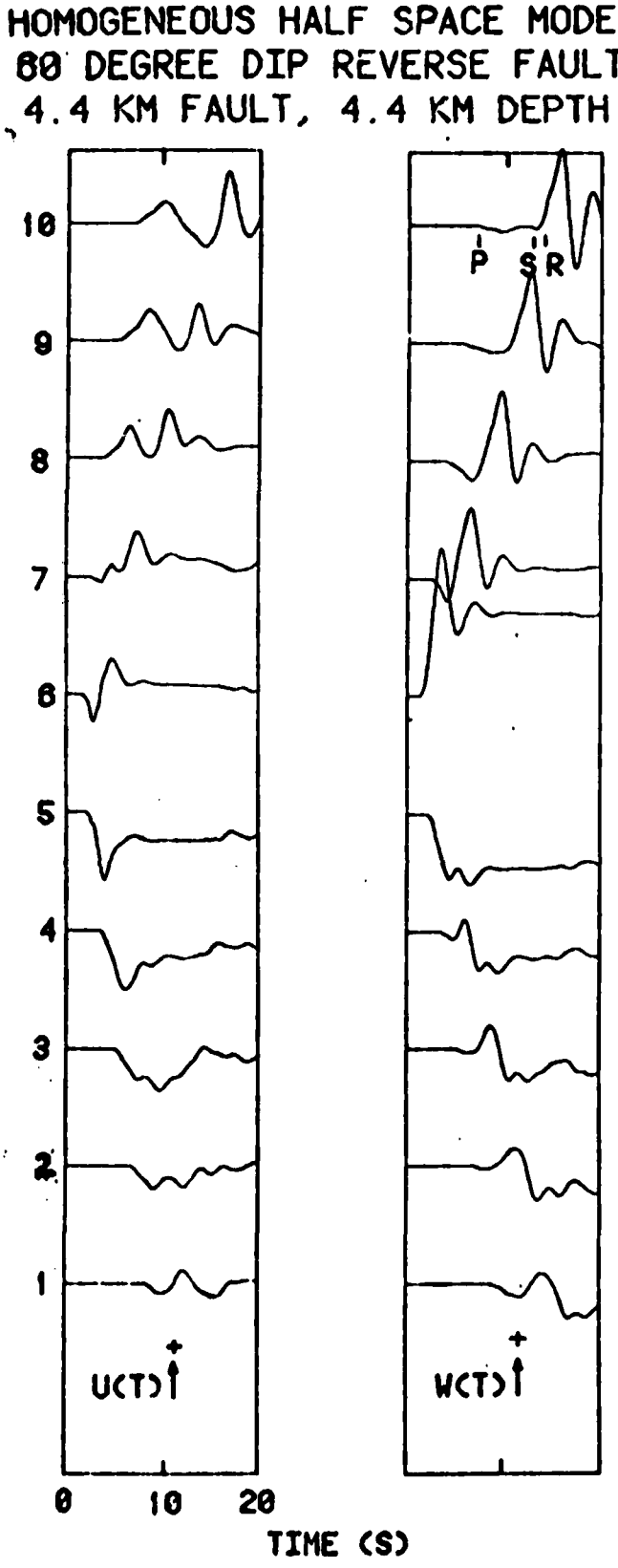

Figure 16. Seismograms (vertical w(t) and radial u(t)) calculated for the model shown in Figure 15.

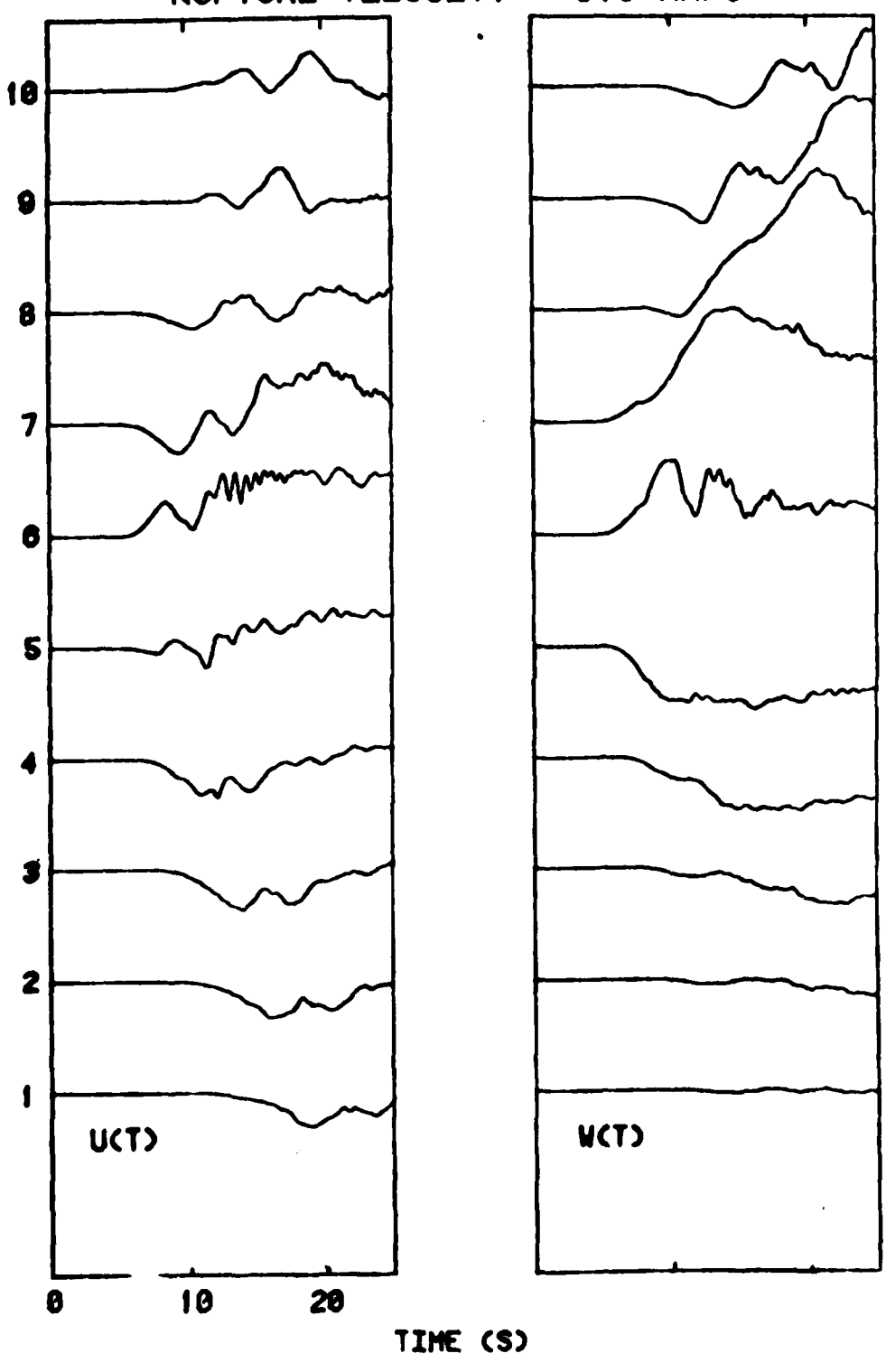

Figure 17. Seismograms calculated for the model shown in Figure 15 except that the source is now a 9.6 km fault at 12 km depth.

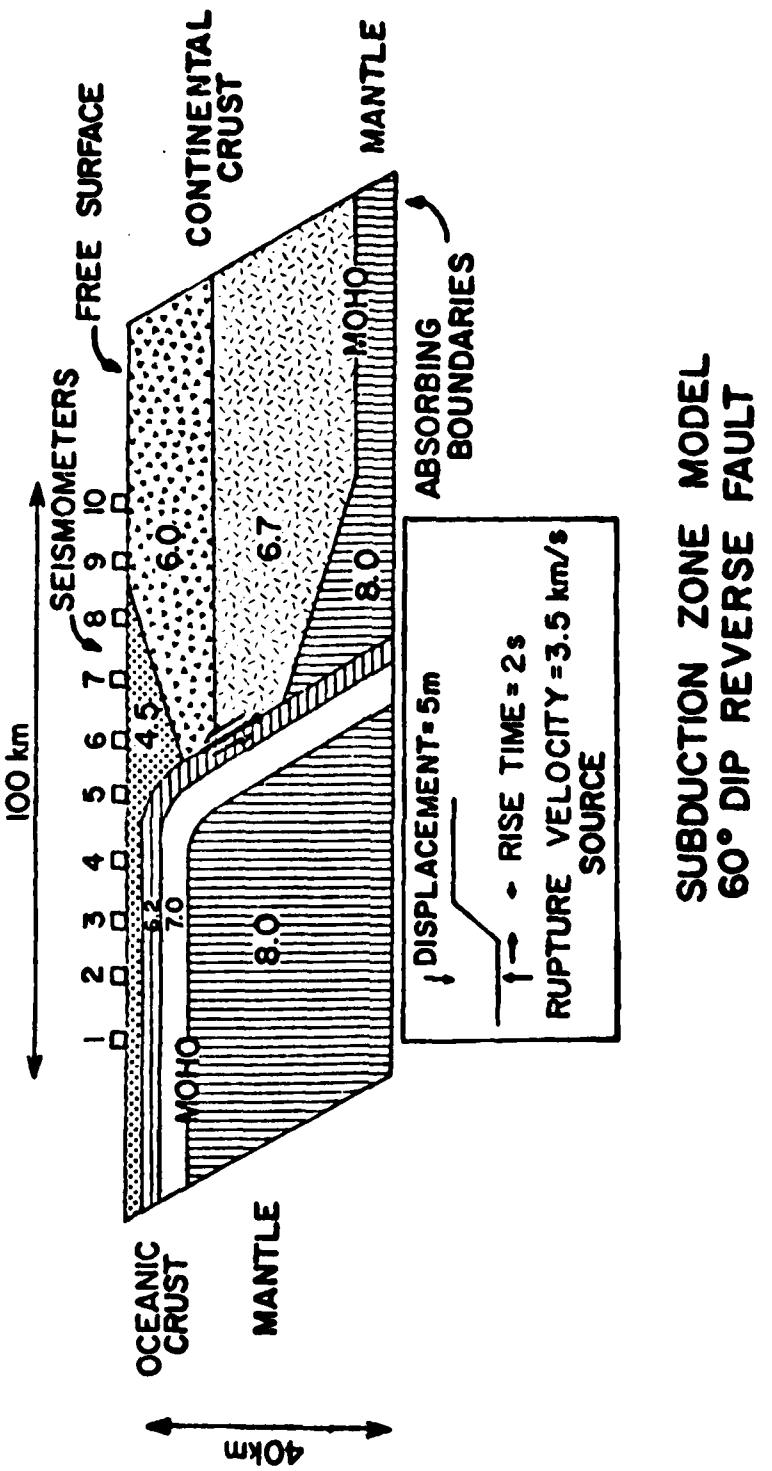

Figure 18. Laterally heterogeneous velocity model with fault (9.6 km long) at 12 km depth.

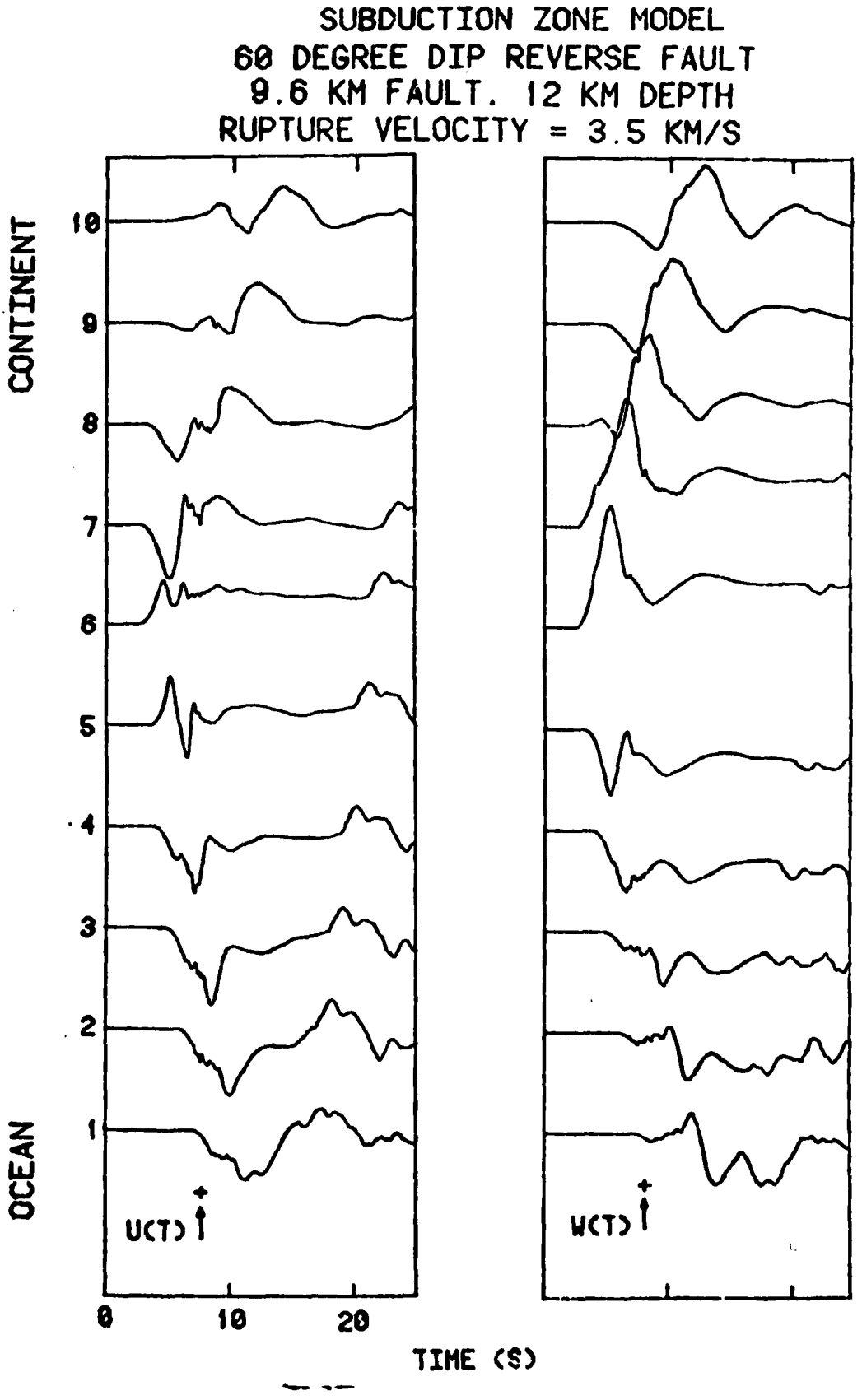

Figure 19. Seismograms calculated for the model shown in Figure 18.

DISTRIBUTION LIST

Chief of Naval Research
Department of the Navy
800 North Quincy Street
Arlington, Virginia 22217
Code 100C1 (1)
Code 460 (1)
Code 463 (5)
Code 480 (1)

ONR Resident Representative
Ohio State Univ. Research Center
1314 Kinnear Road
Columbus, OH 43212 (1)

Director
Naval Research Laboratory
Code 2627
Washington, DC 0375 (6)

Office of Research, Development, Test, and Evaluation
Department of the Navy
Code NOP-987J
Washington, DC 20350 (1)

Director
Defense Advanced Research
Projects Agency
1400 Wilson Boulevard
Arlington, Virginia 22209 (1)

Air Force Office of
Sciencific Research
Department of the Air Force
Directorate of Physics (MPG)
Building 410
Bolling Air Force Base
Washington, DC 20332 (1)

Army Research Office
Department of the Army
Geosciences Division
Box 12211
Research Triangle Park,
North Carolina 27709 (1)

Defense Documentation Center
Building 5
Cameron Station
Alexandria, Virginia 22314 (12)

Procuring Contracting Officer, Code 613
Office of Naval Research
Department of the Navy
800 N. Quincy Street
Arlington, Virginia 22217 (1)

SUPPLEMENTARY DISTRIBUTION LIST

Division of Sponsored Programs (1)
Purdue University
West Lafayette, IN 47907

Prof. James Dorman (1)
Galveston Geophysics Lab of
Marine Science Inst.
University of Texas
Marine Science Inst.
Austin, TX 78712

Dr. George Sutton (1)
Dept. of Geology & Geophysics
University of Hawaii
Honolulu, Hawaii 96822

Dr. Gary Latham (1)
Galveston Geophysics Lab of
Marince Science Inst.
University of Texas
Marine Science Inst.
Austin, TX 78712

Dr. John Kuo (1)
Henry Krumb School of Mines
Columbia University
New York, New York 10027

Dr. Mark Odegard (1)
Earth Physics Program, Code 463
Office of Naval Research
Arlington, VA 22217

Dr. Robert E. Houtz (1)
Lamont-Doherty Geological Obs.
Columbia University
New York, New York 10029

laterally inhomogeneous velocity model.

END